Microsc. Microanal. Microstruct. **8** (1997) 203–225 JUNE **1997**, PAGE 203

X-Ray, Electron Diffraction and HREM studies of $KHTi_4O_9$, xH_2O Thermolysis: Characterization of $K_4Ti_{16}O_{34}$

Maryline Le Granvalet-Mancini ([1]), Anne Marie Marie ([1]), Christian Roucau ([2]), Mayté Caldes ([1]) and Luc Brohan ([1])

([1]) Institut des Matériaux de Nantes, Laboratoire de Chimie des Solides, UMR CNRS 110, Université de Nantes, BP 32229, 44322 Nantes Cedex 3, France
([2]) Centre d'Élaboration de Matériaux et d'Études Structurales, Laboratoire d'Optique Électronique, UPR CNRS 8011, BP 4347, 31055 Toulouse, France

(Received July 17; accepted November 14, 1997)

PACS.61.66.Fn – Inorganic compounds
PACS.61.72.Nn – Stacking faults and other planar or extended defects
PACS.64.70.Kb – Solid-solid transitions

Abstract. — The structure of the new phase $K_4Ti_{16}O_{34}$ was determined from electron diffraction and high resolution electron microscopy data supported by X-ray and thermogravimetric analysis. $K_2Ti_8O_{17}$ obtained from the tetratitanate $K_2Ti_4O_9$ by a soft chemistry reaction transforms at 750 °C into a high temperature form $K_4Ti_{16}O_{34}$. The "cut and projection" method is used to analyze the electron diffraction patterns and to determine the stacking sequences from geometrical feature of the diffraction patterns. The structure deduced from electron diffraction patterns and direct imaging can be described as resulting from a regular intergrowth of two tunnel titanates: the hexatitanate and an hypothetical decatitanate. As the homologous series of tunnels alkali titanates $A_2Ti_mO_{2m+1}$ with $m \geq 6$, the structure is derived from the lepidocrocite archetype. The formation mechanism of the regular block sequence is discussed.

Résumé. — La structure de la nouvelle phase $K_4Ti_{16}O_{34}$ a été étudiée à partir de l'analyse des données de diffraction électronique et microscopie haute résolution, complétée de la diffraction de RX et de l'analyse thermogravimétrique. $K_2Ti_8O_{17}$ obtenu à partir du tetratitanate $K_2Ti_4O_9$ par une réaction de "chimie douce" se transforme à 750 °C sous une forme haute température $K_4Ti_{16}O_{34}$. La méthode de "coupe et projection" est utilisée pour analyser les clichés de diffraction électronique et déterminer les séquences des taches de diffraction à partir de considérations géométriques. La structure, déduite des clichés de diffraction et des images de haute résolution, peut être décrite comme résultant de l'intercroissance de deux titanates à tunnels: l'hexatitanate et un hypothétique decatitanate. Comme les homologues de la série des titanates alcalins adoptant des structures à tunnels $A_2Ti_mO_{2m+1}$ avec $m \geq 6$, celle-ci dérive de la structure archétype lepidocrocite. Le mécanisme de formation de la succession de blocs réguliers est discuté.

1. Introduction

The anhydrous alkali titanates $A_2Ti_mO_{2m+1}$ exhibit layered and tunnel structures and form a homologous series of monoclinic structures [1]. These closely related compounds are described

as long period structures derived from the lepidocrocite type. In the layered titanates, the 1D commensurate modulation of the lepidocrocite framework involves non-conservative antiphase boundaries. Layered structures are observed for $3 \leq m \leq 5$ and tunnel structures for $m \geq 6$.

The host lattices of all the alkali titanates are constructed from zigzag ribbons of octahedra sharing edges. These ribbons are infinite in the b direction. The width of a ribbon in terms of octahedra sharing edges at the same level is $n = m$ for the layered titanates and $n = m/2$ for the tunnel titanates built up from only one type of ribbon. Among the previously described alkali titanates exhibiting a tunnel structure, only $Na_4Ti_{14}O_{30}$ contains two kinds of ribbons, 4 and 3 octahedra in width respectively [2]. The ribbons are joined by octahedra sharing corners to give puckered sheets, present in each n-step titanate, as isolated layers in the lamellar titanates and joined by the available corners in the tunnel structures.

The compound $K_2Ti_8O_{17}$ has been previously prepared from $K_2Ti_4O_9$ by a soft chemistry process involving a $K^+ - H^+$ exchange of one half of the potassium content followed by a topotactic dehydration-condensation reaction while the temperature is increased; this leads to the 3D-octatitanate exhibiting the same framework as the Watts bronze $K_3Ti_8O_{17}$ [3,4].

The present work examines the thermal evolution of $KHTi_4O_9$, xH_2O, the formation of the already known low temperature form of octatitanate (LT) and its transformation at 750 °C into a new form of octatitanate followed by a decomposition at 900 °C into a mixture of anatase and $K_2Ti_6O_{13}$. Powder XRD, HREM and electron diffraction including *in situ* high temperature diffraction measurements and thermogravimetric analysis (TGA) were used in this study.

2. Experimental

The titanate $K_2Ti_4O_9$ was prepared by conventional solid state methods. Stoichiometric quantities of TiO_2 (anatase) and alkali metal nitrates (KNO_3) were ground and pestled to form a pellet. This was then fired in Pt crucible in air at 1000 °C for 1 day. The products were characterized by X-ray powder diffraction (XRD) using a D5000 Siemens diffractometer in a Bragg-Brentano geometry. Acid-exchange of the potassium parent was achieved at room temperature in an aqueous solution. One half of the potassium content was exchanged by immersing the powdered titanate in a stoichiometric amount of 1M HNO_3 for one day. The resulting product was washed with distilled water and finally acetone before drying under vacuum.

The thermogravimetric analysis (TGA) experiments were performed under air with a TGS 2 Perkin-Elmer apparatus at a heating rate of 5 °C/min. The products were analyzed with a TRACOR probe within a 35C Jeol scanning electron microscope.

The relationship between mother phase and final product was determined by least squares refinement of the cell parameters deduced from X-ray powder diffraction data. Transmission electron microscopy (TEM) was used to gather electron diffraction data from both acid-exchanged layered titanates and non hydrated compounds. Electron diffraction investigations were carried out with a Philips CM30, operating at 300 kV. The powder like samples were prepared by grinding under acetone and then deposited on a polymer film supported by a copper grid. High Resolution Electron Microscopy was carried out with a Philips CM30 electron microscope with a point to point resolution of 1.8 Å. Image simulations of high-resolution observations were performed using the Mac Tempas and Crystal Kit programs [5,16].

Table I.

Alkali layered titanates and $Cs_{0.33}TiO_2$			
Compound	n = ribbon width (number of octahedra)	Sequence	Compound plane corresponding to (140) NaCl
$Cs_{0.33}TiO_2$	∞	ABBAC	(130)
$Cs_2Ti_5O_{11}$	5	$(ABBAC)_5AAC$	(001)
$K_2Ti_4O_9$	4	$(ABBAC)_4AAC$	(001)
$Na_2Ti_3O_7$	3	$(ABBAC)_3AAC$	(001)

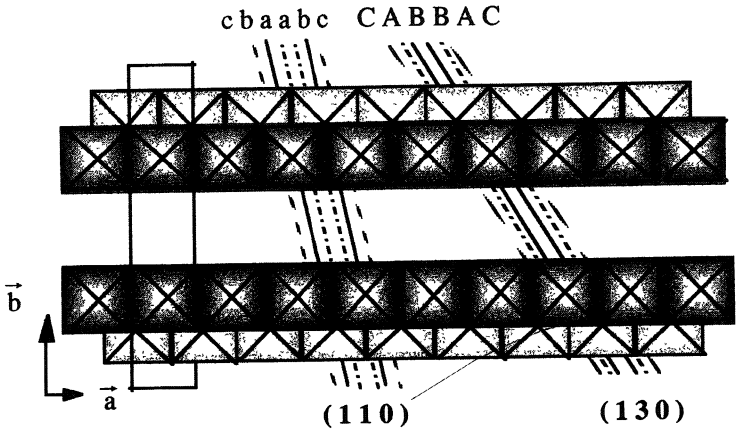

Fig. 1. — Idealized lepidocrocite-type framework projected along [001].

3. Structural Considerations

Commensurate or incommensurate modulated structures have been found quite frequently in condensed matter physics. Among them, long period antiphase boundary structures observed in various binary alloys have been extensively studied [6–9]. In this approach, a basic structure is considered as modulated, *i.e.* divided into "modules" by a set of planar interfaces separated by a constant spacing Δ. A displacement vector **R** is associated with the interface and the modulus of the wavevector of the modulation is $1/\Delta$.

The materials with chemical composition $A_2Ti_mO_{2m+1}$ form a homologous series of compounds in which the framework Ti_mO_{2m+1} is closely related to the lepidocrocite γ-FeO(OH) archetype structure [10]. $Cs_{0.33}TiO_2$ [1] framework belongs to the lepidocrocite type. The latter bronze can be considered as a particular layered titanate with smooth layers, each containing only one ribbon of infinite width. In terms of the rock salt structure this bronze may be formulated as $(Ti_6\square_9)(Cs_2O_{12}\square)$. The titanium-oxygen framework is more precisely described by the sequence ABBAC as indicated in Figure 1 where A, B, C are three kinds of (130) planes. Their compositions in terms of two NaCl-type sublattices are A = [□][O], B = [Ti][O] and C = [□][□]. The (130) lepidocrocite plane corresponds to (140) in the rock salt structure; the sequence for each layered titanate as compared to that of $Cs_{0.33}TiO_2$ is given in Table I.

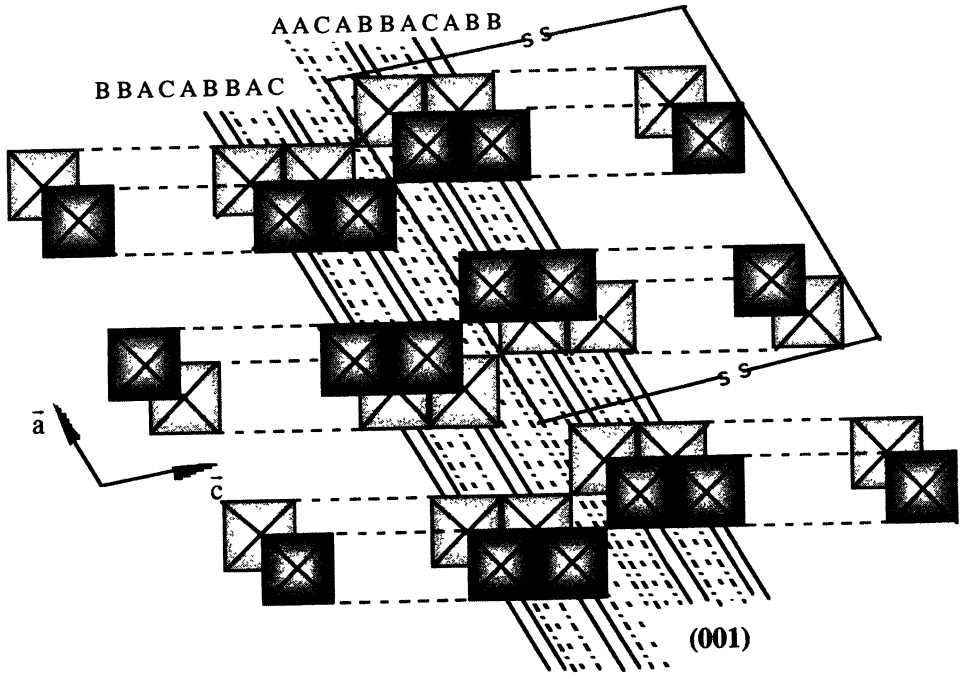

Fig. 2. — Idealized Ti-O framework of alkali layered titanate in projection along [010].

Table II.

Alkali tunnel titanates and $Cs_{0.33}TiO_2$			
Compound	n = ribbon width (number of octahedra)	Sequence	Compound plane corresponding to (230) NaCl
$Cs_{0.33}TiO_2$	∞	abcba	(110)
$K_2Ti_8O_{17}$	4	$(abcba)_4a$	(001)
$Na_4Ti_{14}O_{30}$	4-3	$(abcba)_4a(abcba)_3a$	(001)
$K_2Ti_6O_{13}$	3	$(abcba)_3a$	(001)

All the layered titanates (Fig. 2) can be considered as long period antiphase structures in which the antiphase boundaries are commensurate with the basic lepidocrocite structure. In terms of the lepidocrocite unit cell the translation variant is defined by the displacement vector $\mathbf{R} = \frac{1}{5}$ [010], its modulus being the length of one octahedron edge ($\mathbf{R} = \frac{1}{2}$ [$\bar{1}$10] in terms of the fcc sublattice). Because the displacement vector is not contained in the (130) lepidocrocite antiphase plane, the antiphase is not conservative, two B planes of the sequence ABBAC are suppressed at the antiphase boundaries and the composition of the framework is modified.

Another description of the lepidocrocite framework with which it is more convenient to discuss the tunnel structures (Fig. 3) is given by the sequence (abcba) of (110) planes where a, b, c have the same formula as A, B, C respectively. The (110) lepidocrocite plane corresponds

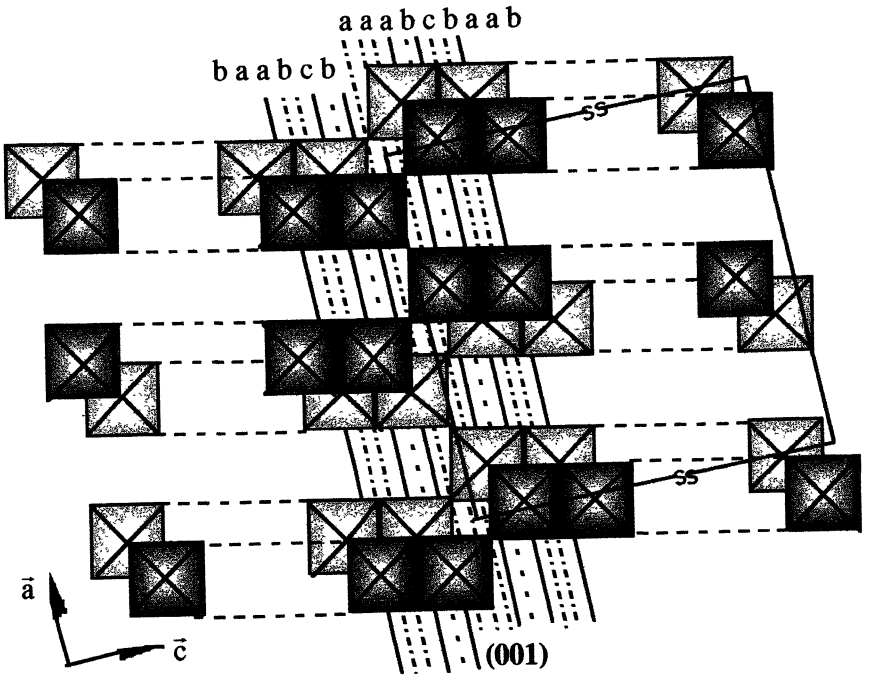

Fig. 3. — Idealized Ti-O framework of tunnel titanates in projection along [010].

to (230) in the rock salt structure. The sequence for each tunnel titanate is indicated in Table II.

This formalism can be used to describe the frameworks of titanates containing M^{II} cations such as $A_2M^{II}Ti_{10}O_{22}$ with A = Na, K, Rb and M^{II} = Ba, Sr, Pb [11, 12] (Fig. 4). The full stacking symbol of this compound would for instance be: [(**abcba**)$_3$**a**(**abcba**)$_2$**a**]. The framework of a hypothetical tunnel tetratitanate could be written (**abcba**)$_2$**a**. Although such a titanate has not yet been isolated, it exists as an intergrowth with the hexatitanate (**abcba**)$_3$**a** in the framework of $A_2M^{II}Ti_{10}O_{22}$.

Another example of such intergrowths is given by the tunnel titanate $Na_4Ti_{14}O_{30}$ which can be considered as built from hexa and octa titanates. In all these intergrowths, the difference in width between two adjacent ribbons is only one octahedron. In the second part of this paper is described a new form of $K_2Ti_8O_{17}$ exhibiting a difference of *two* octahedra between adjacent ribbons. Before describing the idealized structure of the high temperature phase of $K_2Ti_8O_{17}$ it may be of interest to briefly discuss the origin of the superstructure spots observed on the electron diffraction patterns.

4. Interpretation of the Diffraction Patterns

In physical space, the shear structure is the convolution product of the superlattice generated by the shearing operation with a slab of the basic structure (the lepidocrocite in the case of the alkali titanates). The diffraction pattern is then the Fourier transform of this convolution product, *i.e.* the ordinary product of two Fourier transforms: the reciprocal lattice of the shear structure and the Fourier transform of a basic structure slab. The latter can be obtained

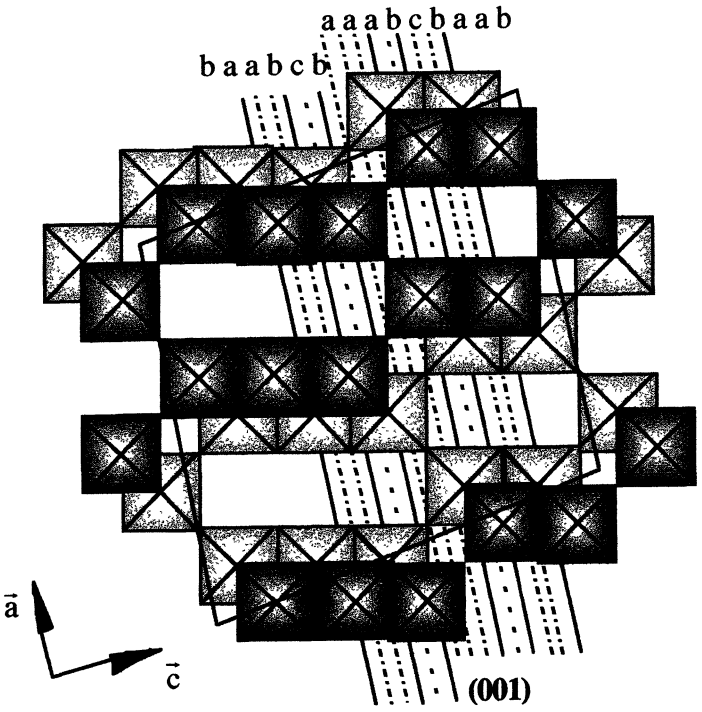

Fig. 4. — Idealized Ti-O framework of titanates containing M^{II} cations such as $A_2M^{II}Ti_{10}O_{22}$ in projection along [010].

as follows: since in physical space a basic structure slab is the ordinary product of the basic structure with the window function limiting the slab, the transform of such a slab is the convolution product of the reciprocal lattice of the basic structure with the window transform.

The **q** modulation wave vector is $1/m$ $[001]^*$ = $1/n$ $[001]^*$ for layered titanates and $2/m$ $[001]^*$ = $1/n$ $[001]^*$ for tunnel titanates built up from only one type of ribbon. Moreover, in the case of titanates built up from only one sort of ribbons, it can be noted that the satellite spot intensities are identical. Some examples of diffraction patterns of alkali titanates $A_2Ti_mO_{2m+1}$ are given in Figures 5 and 8. The $[\bar{1}10]$ electron diffraction pattern of $K_2Ti_6O_{13}$ is shown in Figure 5. The separation of the basic spots along $[001]^*$ (corresponding to the thickness of one TiO_6 octahedra) is divided into three equal intervals by the diffraction spots. The interspot spacing reveals directly the average block size. Since the separation of the first relatively intense spot from the basic spot is given by the vector $\mathbf{q} = 1/3$ $[001]^*$, the ribbon's width (number of octahedra) is $n = 3$ and consequently m is equal to 6.

The long lattice parameter of the superstructure is $\mathbf{c} = n\mathbf{a}$ where **a** is a parameter of the lepidocrocite unit cell. In the case of tunnel titanates containing two sorts of ribbons, n in the preceding expressions is replaced by $n_1 + n_2$ where n_1 and n_2 are the widths of the component ribbons. In the general case, the average widths of the ribbons must be equal to the average block size, which is given by $[n_1p + n_2q]/(p + q)$, where p and q are the numbers of n_1 and n_2 blocks respectively. In other words, $p/(p + q)$, and $q/(p + q)$, are the relative abondancies of the two block types.

Fig. 5. — Diffraction pattern along the $[\bar{1}10]$ zone axis of $K_2Ti_6O_{13}$.

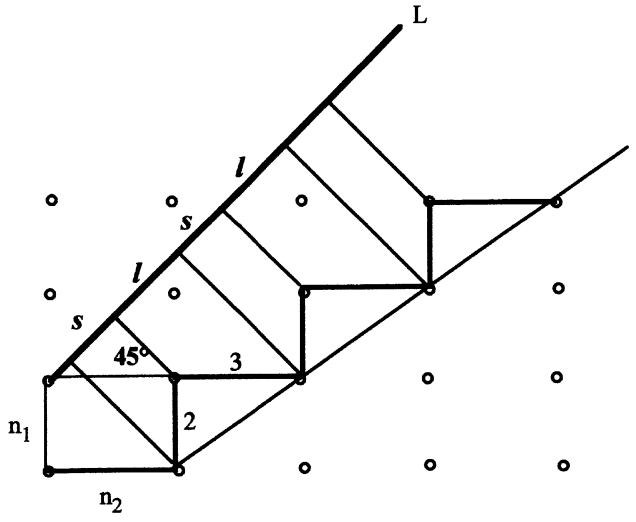

Fig. 6. — "Cut and projection" method applied to the derivation of the stacking sequence 2-3 in $K_2SrTi_{10}O_{22}$.

The "cut and projection" method is a simple example of "embedding" a non periodic structure (1D) in a higher dimensional space (2D) in order to make it periodic [9, 13, 14]. It is possible to map each block sequence on a 2D lattice with a rectangular unit mesh of $n_1 \times n_2$ units. Assuming the number of n_1 layer blocks to be plotted along the vertical direction and the number of n_2 layer blocks in the horizontal direction, any sequence consisting of the two types of block is thus imaged as a zigzag path on this 2D lattice. The sequence which best approximates a uniform distribution of ribbons is then represented by the zigzag line which fits best the straight line S. The slope is given by the ratio of the total length of the ribbons sequences along the two directions (Fig. 6).

$$\tan \varphi = n_1 p / n_2 q.$$

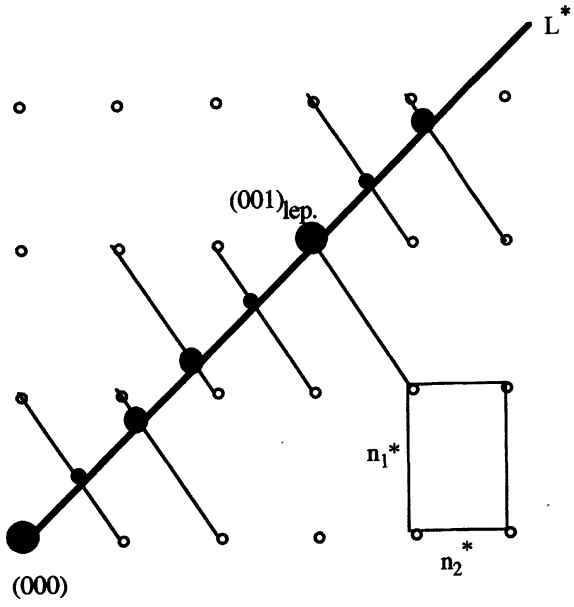

Fig. 7. — Theoretical diffraction pattern of the phase $K_2SrTi_{10}O_{22}$ using the "cut and projection" method.

The stacking sequences of long **l** and short **s** spacings can be obtained by projecting the zigzag line within the strip onto a line L with a slope of 45° with the horizontal.

As an example the sequence leading to the composition $K_2SrTi_{10}O_{22}$ is shown Figure 6 in which $n_1 = 2$, $n_2 = 3$ and $p = q = 1$. The 2D lattice consists of rectangles of 2×3 units and the slope of the slits given by $\tan \varphi = 2/3$.

The application of a variant of the "cut and projection" method makes it possible to deduce not only the stacking sequence but also the essential features of the diffraction patterns for given values of n. The diffraction pattern is obtained by the transformation to the Fourier space of the different operations giving rise to the strip. Every node of the reciprocal lattice is replaced by a line perpendicular to the strip. The strip onto the line L corresponds in reciprocal space with the intersection with the line L^*. Scattering then occurs at the intersection points of the line L^* with the projection lines perpendicular to the slit direction through the reciprocal lattices nodes. The relative intensities of the diffraction spots, represented by dots of different sizes decrease rapidly with the distance between the node and the line L^*.

Figure 7 shows for instance the pattern to be expected for the 2-3 sequence in $K_2SrTi_{10}O_{22}$. The geometry and the relative spot intensities are found to correspond remarquably well with the observed ones (Fig. 8). Inversely, the block sequence and therefore the composition can be deduced from such diffraction pattern. The distance between two successive basic spots is divided into 5 equal intervals: the average modulation vector is $\mathbf{q} = 1/5\ [001]^*$, consequently $n = 5$ and $m = 10$. The first intense spot, counted from the basic spots is the second one; this means that $n_1 = 2$ and thus $n_2 = 3$. In this case, two subsequent blocks do not differs from more than one octahedra.

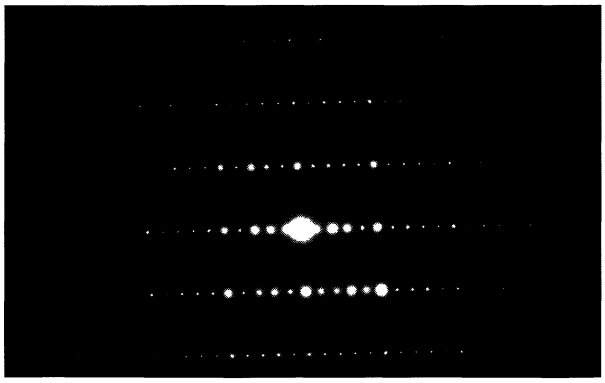

Fig. 8. — Diffraction pattern of the phase $K_2SrTi_{10}O_{22}$; the direction [001]* can be compared with Figure 7.

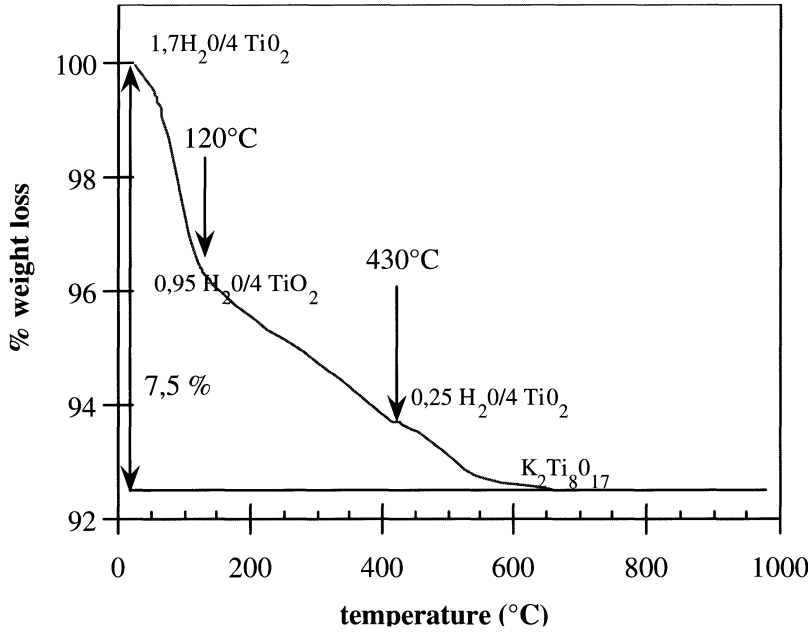

Fig. 9. — Thermogravimetric analysis curve of the exchanged compound $KHTi_4O_9$, xH_2O obtained from $K_2Ti_4O_9$.

5. Thermolysis Study

The thermogravimetric analysis (TGA) experiments were performed under air. The exchange rate was checked by semi-quantitative analysis in a 35C Jeol scanning electron microscope equipped with a TRACOR probe. At the end of the treatment, the exchange rate is close to 50%.

The TGA curve is shown in Figure 9. It reveals a monotonous weight loss which is achieved at 650 °C. The XRD pattern of the final compound obtained at 700 °C is characteristic of the octatitanate $K_2Ti_8O_{17}$.

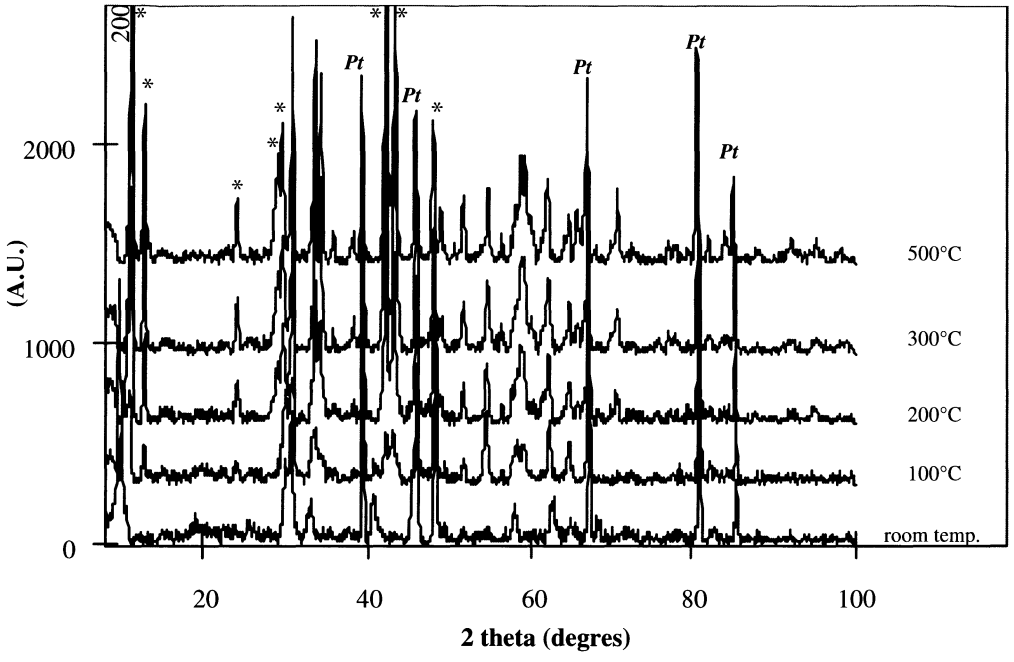

Fig. 10. — Powder X-ray diffraction patterns of exchanged titanate $KHTi_4O_9$, xH_2O in temperature range 25-500 °C.

Since the final product is known and because all the weight loss can be associated to a water departure, the exchanged product can be expressed $KHTi_4O_9$, $0.95H_2O$ at 120 °C. The slope change observed around 430 °C corresponds then to the global composition and $KHTi_4O_9$, $0.25H_2O$.

At 900 °C, the XRD pattern reveals that the octatitanate decomposed into a mixture of TiO_2 anatase and $K_2Ti_6O_{13}$.

6. X-Ray Diffraction

In the temperature range 25 to 500 °C, X-ray patterns of the anhydrous compound exhibits a sharp relationship with the pattern of the exchanged compound as shown in Figure 10.

The $K_2Ti_8O_{17}$ diffraction peaks (indicated by an "asterisk"), appear at 100 °C then their intensities increase with the temperature. The $KHTi_4O_9$, xH_2O d_{h00} intensities characteristic of the interlayer spacing continuously decreases between 100 °C and 500 °C. As can be seen in Table III, in which are compared the cell parameters of the starting 2D-material with those of the 3D-octatitanate, the c parameter characteristic of the ribbon width and the b parameter do not change in this temperature range whereas the a and β parameters decrease.

The main conclusion for this study is that the evolution of the 2D-phase to the 3D $K_2Ti_8O_{17}$ takes place in a progressive way. According to the particular structural relationship between the hydrolysis compound and the octatitanate — *i.e.* the conservation of zig-zag ribbons — this evolution could be explained by a condensation of zig-zag ribbons of octahedra edges which involves the formation of near-periodic sequences along **a**. This suggests that the water

Table III. — *Refined cell parameters of* $KHTi_4O_9$, xH_2O *and* $K_2Ti_8O_{17}$.

	a (Å)	b (Å)	c (Å)	β (°)	space group
$KHTi_4O_9$, xH_2O	18.42(1)	3.754(2)	12.01(1)	106.10(7)	C 2/m
$K_2Ti_8O_{17}$	15.79(1)	3.804(2)	12.052(8)	96.02(4)	C 2/m

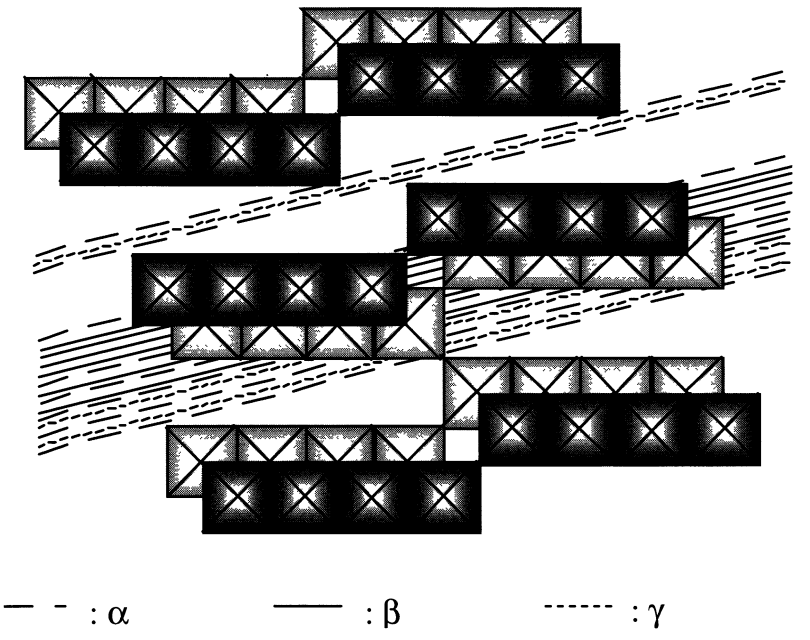

Fig. 11. — Idealized Ti-O framework of alkali titanates in projection along [010] which shows the topotactic formation of the tunnel structure $K_2Ti_8O_{17}$ by condensation of two $[K(H_2O)Ti_4O_7(OH)]$ layers.

departure and the dehydroxylation process take place simultaneously. The proposed structural model is shown in Figure 11.

In order to describe this condensation it is convenient to write the starting material and the octatitanate Ti-O frameworks in terms of (100) planes as $\gamma(\alpha\gamma)_2(\alpha\beta)_3\beta_2(\beta\alpha)_3(\gamma\alpha)_2$ and $\gamma(\alpha\gamma)_2(\alpha\beta)_3\beta_2(\beta\alpha)_3(\gamma\alpha)$ respectively where α, β, γ have the same composition as A, B, C respectively (Fig. 11).

The condensation results in the formation of periodic antiphase (100) planes. For two successive antiphase planes the displacement vectors are $\mathbf{R}_1 = \frac{2}{45}\,[\bar{1}05]_{M_2Ti_4O_9}$ and $\mathbf{R}_2 = \frac{2}{45}\,[10\bar{5}]_{M_2Ti_4O_9}$ respectively, *i.e.* $\frac{1}{2}\,[110]_{fcc}$ and $\frac{1}{2}\,[\bar{1}\bar{1}0]_{fcc}$. Their modulus is the length of one octahedron edge. The displacement vectors are not contained in the antiphase (100) planes, therefore the antiphases are not conservative. One $\gamma\alpha$ pair of planes is suppressed at each antiphase boundary and the composition of the Ti-O framework is modified.

The intermediates states can be formulated as the following:

$$[K(H_2O)Ti_4O_7(OH)]_{1-y},\quad (K_2Ti_8O_{17})_{y/2}\quad \text{with}\quad 0 \leq y \leq 2.$$

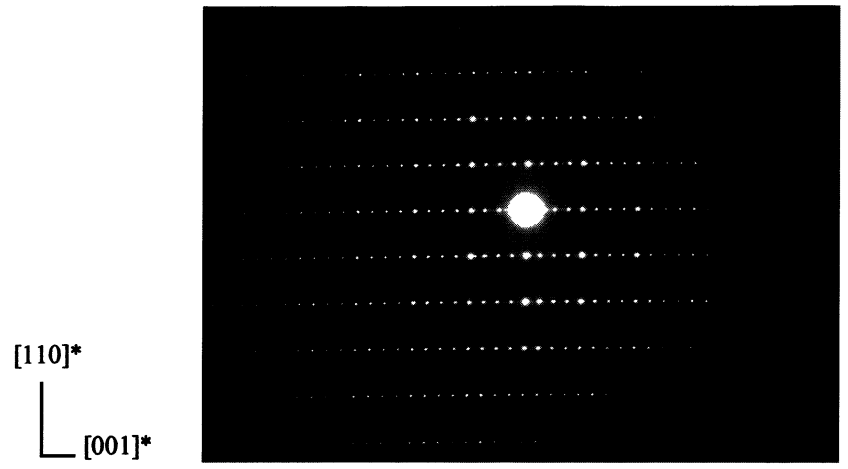

Fig. 12. — [$\bar{1}$10] zone axis electron diffraction pattern of $KHTi_4O_9$, xH_2O. The superlattice reflections along c^* correspond to $n = 4$ (octahedra width of the ribbon).

$K_2Ti_8O_{17}$ is stable up to 700 °C and decomposes at 900 °C into a mixture of $K_2Ti_6O_{13}$ and TiO_2 anatase. A new intermediate phase was characterized by electron diffraction and high resolution electronic microscopy (HREM).

7. Electron Diffraction

At room temperature, the [$\bar{1}$10] diffraction pattern for $KHTi_4O_9$, xH_2O exhibits 3 superstructure spots along $\mathbf{c}^*$ (Fig. 12). These spots are attributable to the 2D skeleton composed of 4 octahedron along $\mathbf{c}$. In the case of titanates built up from only one sort of ribbon, it can be noted that the satellite spot intensities are identical.

The observed reflections ($hk0$), with $h + k = 2n$ suggest a C-centered structure for $KHTi_4O_9$, xH_2O. Since for the $K_2Ti_8O_{17}$ and $KHTi_4O_9$, xH_2O compounds the dimension of the ribbons are quite similar — *i.e.* the b and c parameters (Tab. III) — the spots position along the [001]* direction of [$\bar{1}$10] zone axis E.D. pattern do not change from ambient temperature to 600 °C.

During the *in situ* heating, additionnal reflections observed in the [001]* direction E.D. pattern suggest that an irreversible transformation appears in the temperature range 730 °C–750 °C. In the [$\bar{1}$10] zone axis electron diffraction pattern for the HT $K_2Ti_8O_{17}$ (Fig. 13), the distance between two successive basic spots is divided into 8 equal intervals along [001]*: the modulation vector is $\mathbf{q} = 1/8$ [001]*. Assuming that the tunnel structure is maintained ($\mathbf{q} = 2/m$) and that the ratio K/Ti = 1/8 is retained, the composition can be expressed as $K_4Ti_{16}O_{34}$. The first intense spot, counted from the basic spots is the third one; this means that $n_1 = 3$ and therefore $n_2 = 5$ since $n_1 + n_2 = n$.

Using the "cut and projection" method previously described, the block sequence corresponding with this value of q is 35 (Fig. 14). Also the theoretical diffraction pattern can be deduced graphically; the result is shown in Figure 15. The relative intensities of the spots are quite well reproduced, as can be judged by comparing with Figure 13.

The block sequences and thus the antiphase boundaries are directly observed in high resolution microscopy images along $\mathbf{c}$ direction.

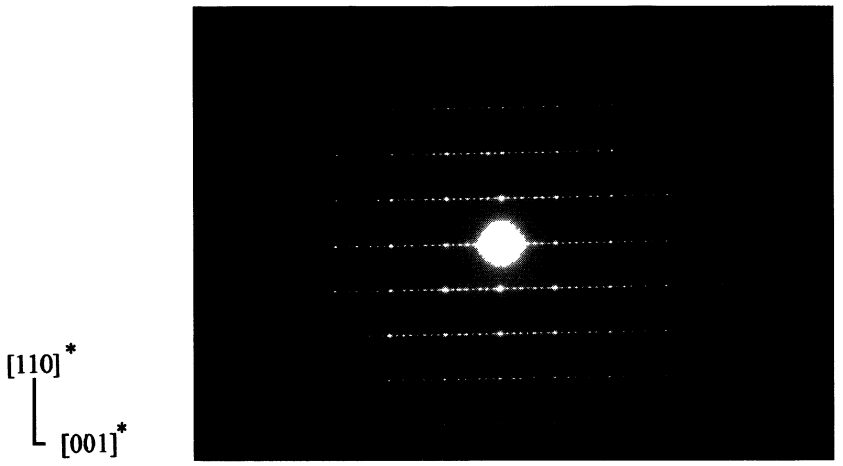

Fig. 13. — [$\bar{1}$10] zone axis electron diffraction pattern of HT $K_2Ti_8O_{17}$.

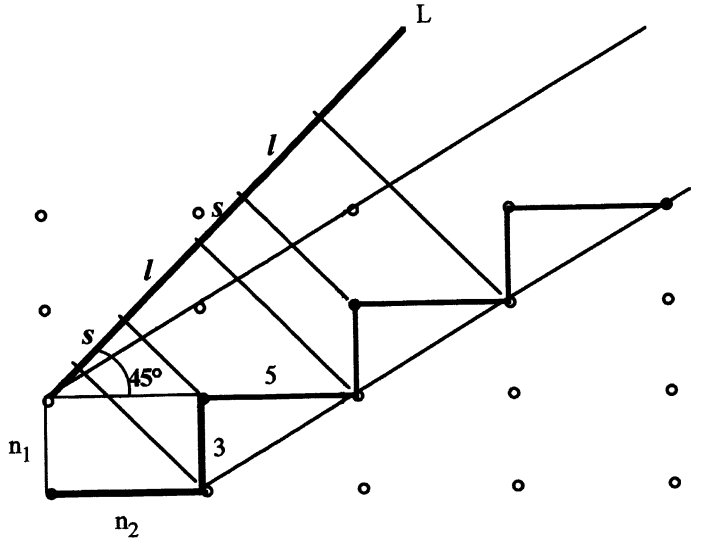

Fig. 14. — "Cut and projection" method applied to the 3-5 intergrowth of $K_4Ti_{16}O_{34}$.

8. High Resolution Electron Microscopy

High resolution images of titanate structure can be obtained along the [$\bar{1}$10] section, since in these sections, satellites due to modulation are present. The result is shown in Figure 16 for $KHTi_4O_9$. In [$\bar{1}$10] HREM image, only the $n = 4$ type modulation along **c** is present, which is characterized by antiphase boundaries predominantly located on the double AA layers (Ti vacancies: see Fig. 2). The enlarged experimental and calculated (included as an inset) HREM images along [$\bar{1}$10] are shown in Figure 18. The structural model of $KHTi_4O_9$ is deduced from the previously reported isostructural layered titanate [15] in which the K cations are statistically distributed on the Wyckoff positions 4i and 2d — *i.e.* oxygen vacancies sites —

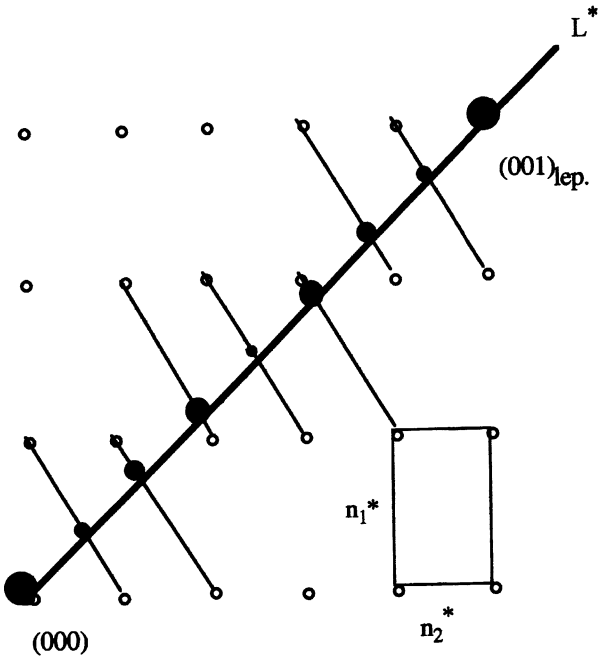

Fig. 15. — Graphical method to determine the approximate relative intensity distribution in the diffraction pattern of $K_4Ti_{16}O_{34}$.

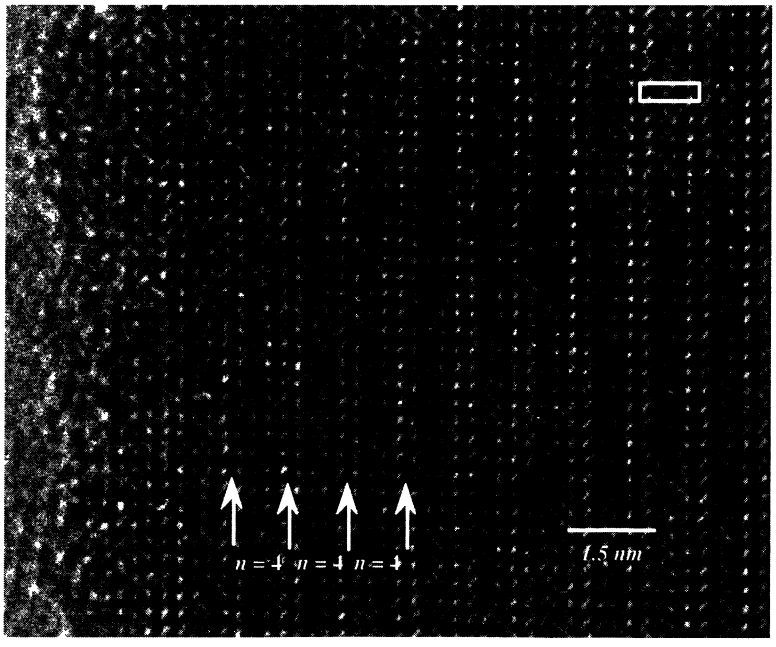

Fig. 16. — [$\bar{1}$10] HREM image for $KHTi_4O_9$: the $n = 4$ spacing appears as regular black contrast along **c** (see white arrows).

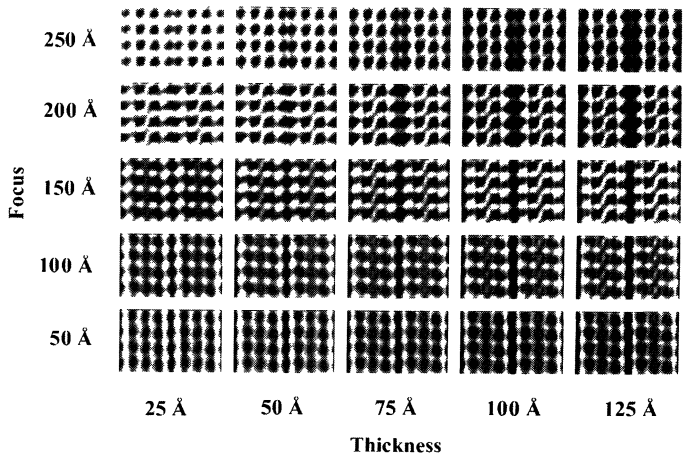

Fig. 17. — Through-focus series of $KHTi_4O_9$: focus step 50 Å, thickness step 25 Å.

in C2/m space group. As it can be seen in Figure 17, the best simulation is obtained at defocus of 150 Å and for a crystal thickness of 25 Å. A good match has been achieved between this simulation and the experimental image; therefore the white dots in Figure 18 correspond to Ti-O columns while the black contrasts are associated to the K cations. One easily recognizes the stacking of the $n = 4$ atomic blocks according to the sequence $(ABBAC)_4AAC$ with the repeat unit of about 12 Å along the **c** direction.

The result of the X-ray diffraction experiment is confirmed by the *in situ* heating of the $KHTi_4O_9$ sample in the microscope. At temperature of about 600 °C an irreversible transformation appears without changing the superstructure reflections number. The [$\bar{1}$10] HREM observed image as well as the structural model of LT $K_2Ti_8O_{17}$ are shown in Figure 19. The crystal structure data used for the image simulation was previously reported by Sasaki *et al.* [16]. The K ions are randomly distributed on the two Wyckoff positions 4i. In order to improve the experimental contrast, one part of the crystal was filtered. The experimental contrast observed fits quite well with the calculated one for a defocus of −600 Å and for a crystal thickness of 50 Å (Fig. 20). The spacing between two **a**-type layers is limited by white dots rows enclosing the doubleTi-O columns which appear as four elongated dark dots.

According to the structure proposed for the HT $K_2Ti_8O_{17}$ form in previous paragraphs, the [$\bar{1}$10] HREM image shown in Figure 21 reveals a regular 3-5 intergrowth along **c**. In the structural model presented along the projecting directions [$\bar{1}$10] (Fig. 21) and [001] (Fig. 23), the K cations are statistically distributed on oxygen vacancies positions which are located in the **c**-type plane. On the simulated image, lower electron density zones appear as a white dots therefore atoms are located on dark contrast zones. The good agreement between the experimental image and the simulated one (Fig. 22) (focus −850 Å and thickness 180 Å) allows us to concluded that the high temperature form of the octatitanate is built up from a complex sequence consisting of two blocks of 3-steps and 5-steps tunnels titanates respectively (Fig. 23). The full stacking symbol of this compound would be $[(\mathbf{abcba})_5\mathbf{a}(\mathbf{abcba})_3\mathbf{a}]$ in that way the modulation can be regarded as a periodic arrangement of **a**-type plane.

In the HT octatitanate, the average distance between subsequent **a** regions should be about 3-5 basic units (let 24 Å) along the c direction. However, as can be seen from the [$\bar{1}$10] HREM image (Fig. 24), a variety of modulation vectors may locally occurs. One can locally detect

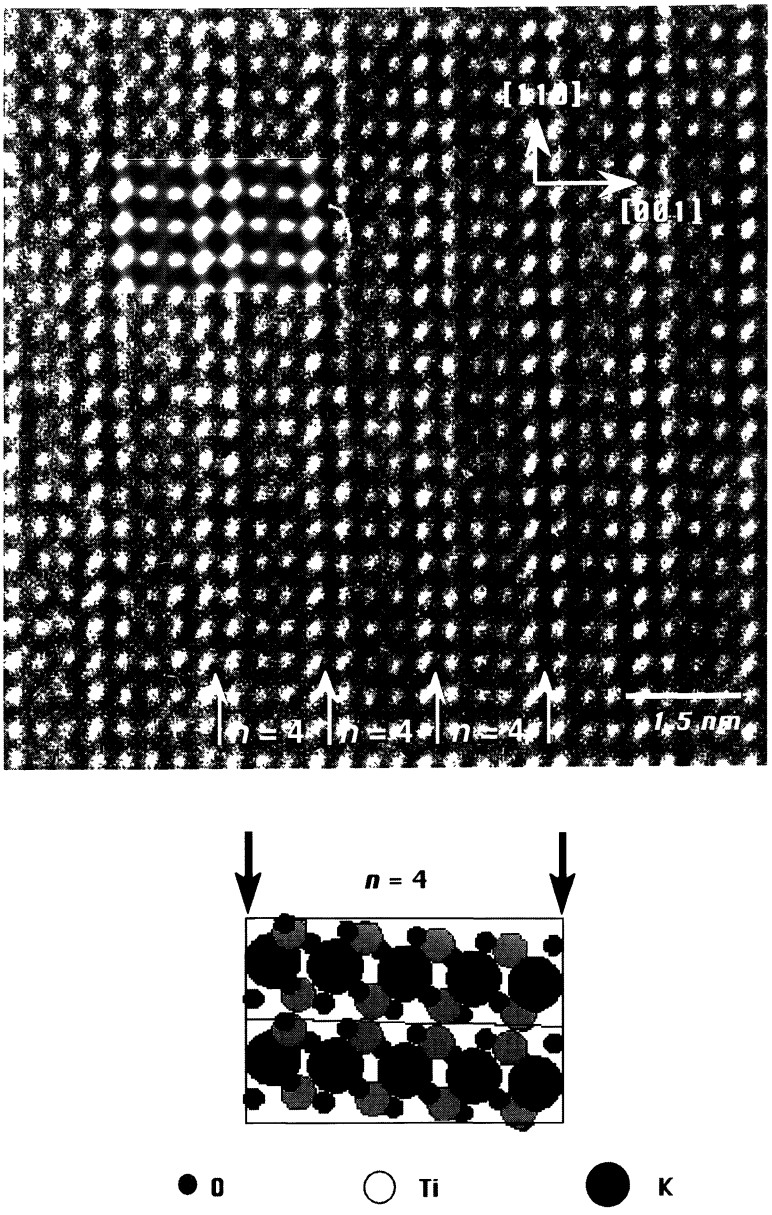

Fig. 18. — a) Enlarged [$\bar{1}$10] HREM image of $KHTi_4O_9$. Calculated image is show as an inset (focus 150 Å and thickness 25 Å). b) Schematic model of $KHTi_4O_9$: $n = 4$ spacing appears on the AA layers.

deviations from the C-centering; Figure 24 is consistent with a mixture of both LT and HT octatitanate forms.

In contrast to the C centered unit mesh observed for HT octatitanate (Fig. 21), a primitive unit mesh, *i.e.* a non centered unit mesh, is far more abundant in the crystal edge. The simulation is based on the model of Figure 24 (bottom) built from $n = 4$, $n = 5$ and $n = 3$ successive sequences, at focus −700 Å and for crystal thickness of 50 Å (Fig. 25): the white dots

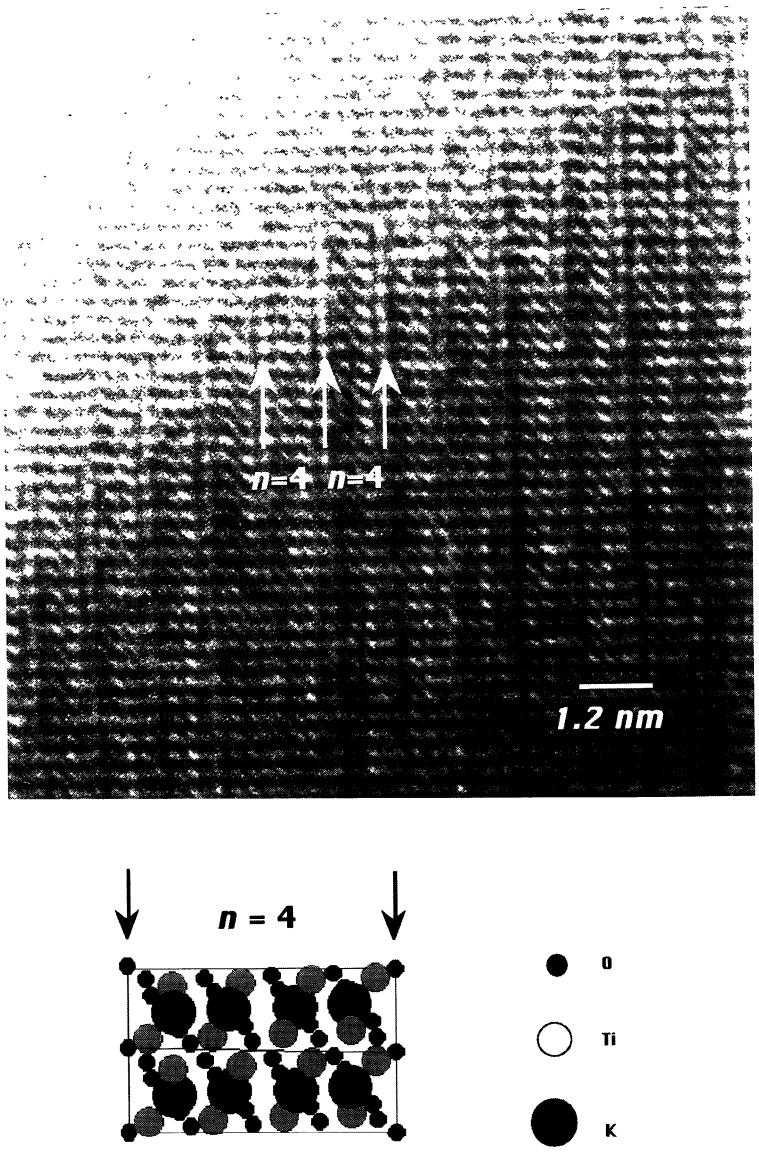

Fig. 19. — a) HREM image of LT octatitanate for [$\bar{1}$10] zone axis. b) Schematic model of LT octatitanate: $n = 4$ spacing appears on the **a**-type layers (white dots).

correspond to the lower electron density zones between atom columns. The good agreement between experimental and simulated images, allows us to propose a schematic model (Fig. 26) for the LT to the HT octatitanate transformation. As mentioned above, the HT $K_2Ti_8O_{17}$ long period can also described by a repetition of a composite sequence, $(\mathbf{abcba})_3\mathbf{a}(\mathbf{abcba})_5\mathbf{a}$. In comparison to the $(\mathbf{abcba})_4\mathbf{a}$ sequence of LT $K_2Ti_8O_{17}$, its appears that the transformation results in a shift of one upon two interface boundaries in such way that the composition is not modified. The modulus of this shift is one octahedron edge [17].

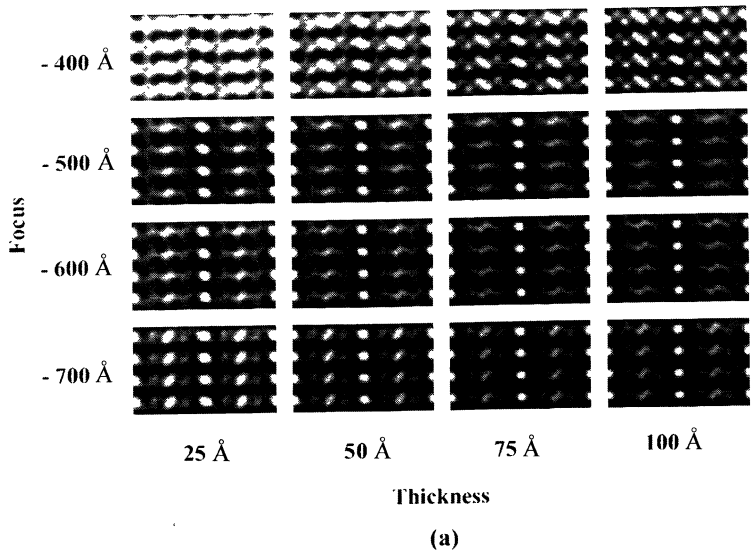

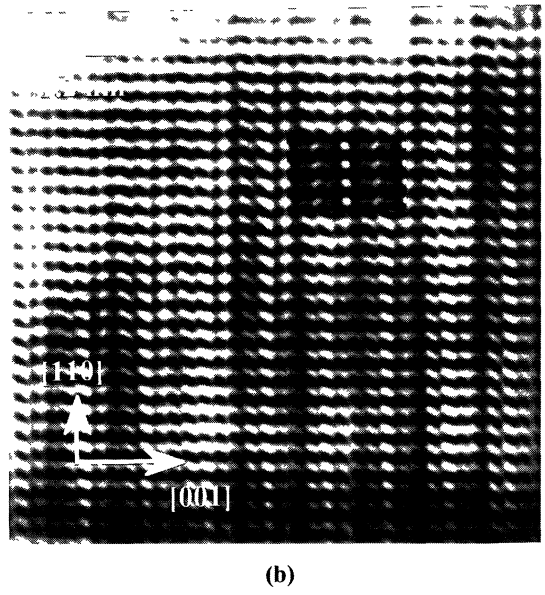

Fig. 20. — a) Through-focus series of LT octatitanate: focus step 100 Å, thickness step 25 Å. b) filtered [$\bar{1}$10] HREM image of LT octatitanate: calculated image is included as an inset (focus −600 Å, thickness 50 Å).

9. Conclusion

The anhydrous alkali titanates $A_2Ti_mO_{2m+1}$ form a homologous series of monoclinic structures. The framework of both layered and tunnel titanates Ti_mO_{2m+1} is closely related to

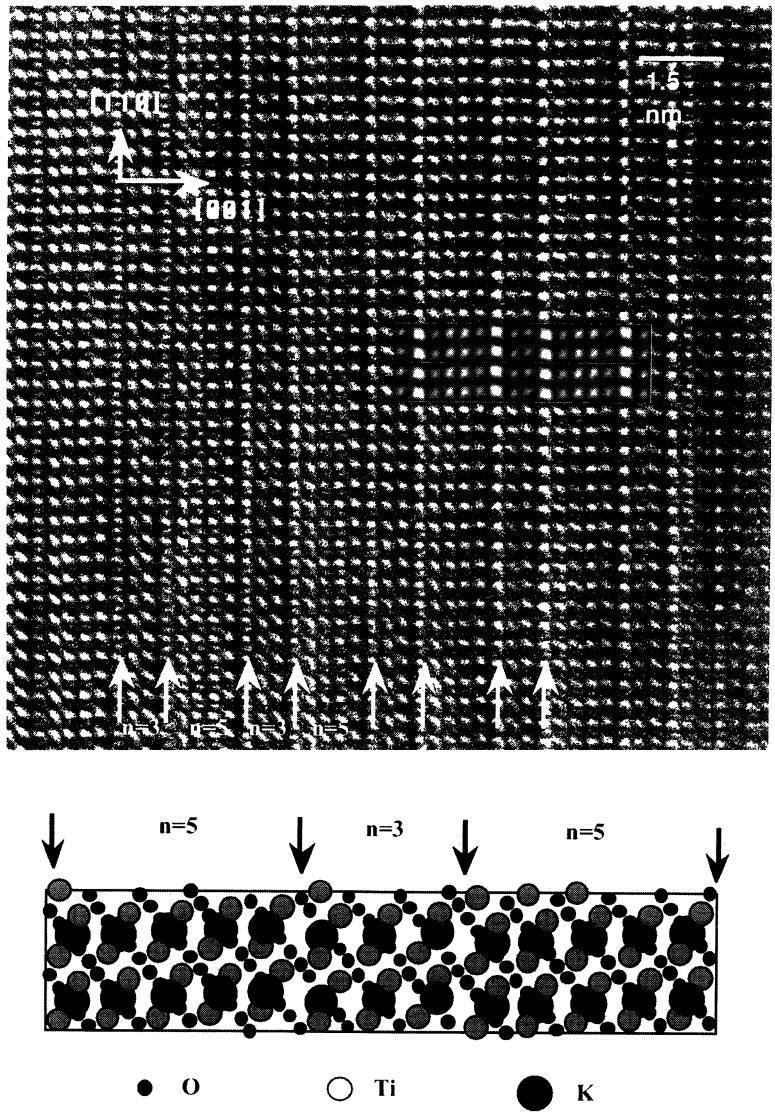

Fig. 21. — [$\bar{1}$10] HREM images of HT octatitanate crystal showing $n = 3$ and $n = 5$ intergrowth along **c**. Calculated image is included as an inset (focus −850 Å and thickness 180 Å).

the lepidocrocite γ-FeO(OH) archetype structure. It can be described as long period structures derived from the lepidocrocite type.

For the layered titanates $3 \leq m \leq 5$, there is a 1-D commensurate modulation involving non-conservative antiphase boundaries. Because the displacement vector is not contained in the (130) lepidocrocite antiphase plane, the antiphase is not conservative and the composition of the framework is modified.

In the case of tunnel titanates for $m \geq 6$, there are two commensurate modulations. The first one is the same as in the layered titanates and leads to puckered sheets. The second one

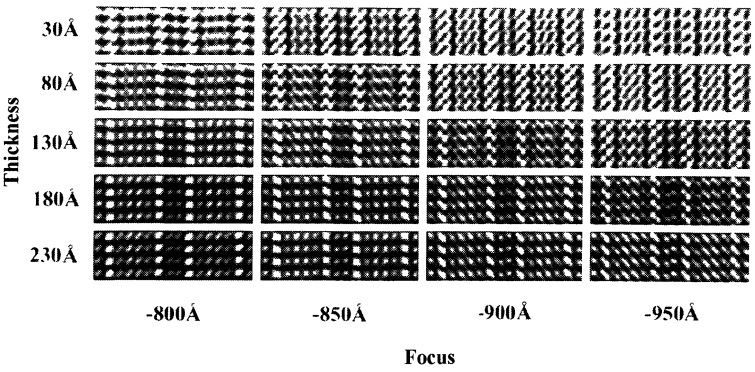

Fig. 22. — Through-focus series of HT octatitanate: focus step 100 Å, thickness step 50 Å.

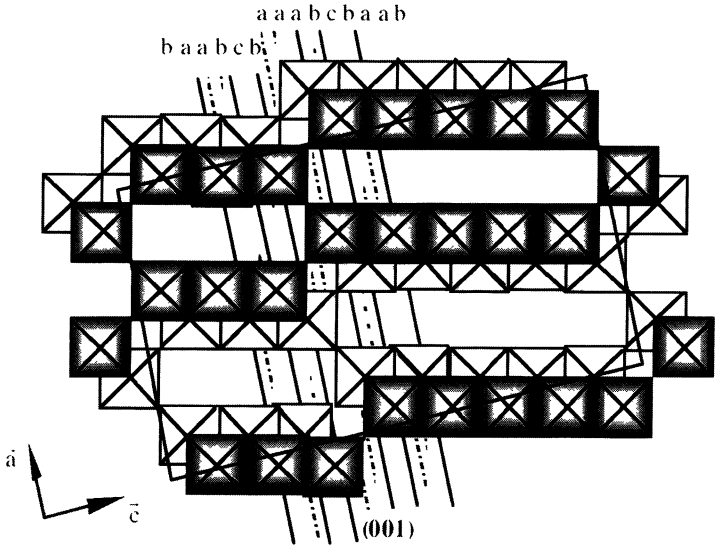

Fig. 23. — Idealized Ti-O framework of the HT $K_2Ti_8O_{17}$ in projection along [010].

concerns the condensation of the sheets to give a tunnel framework. It involves non conservative antiphase boundaries along the [100] titanate axis.

These titanates built up from only one sort of ribbons, exhibit satellite spot whose the intensities are identical and for which the **q** modulation wave vector is $1/m$ [001]* for layered titanates and $2/m$ [001]* for tunnel titanates. The long lattice parameter of the superstructure is $\mathbf{c} = n\mathbf{a}$ where **a** is a parameter of the lepidocrocite unit cell. The application of a variant of the "cut and projection" method makes it possible to deduce not only the stacking sequence but also the essential features of the diffraction patterns for given values of n. Inversely, the block sequence and therefore the composition can be deduced from diffraction pattern.

The HT $K_2Ti_8O_{17}$ form exhibits these two types of modulation, leading to the intergrowth of two tunnel titanates with steps differing from more than one octahedron. Using the "cut and projection" method, the block sequence corresponding with this value of **q** is 3-5.

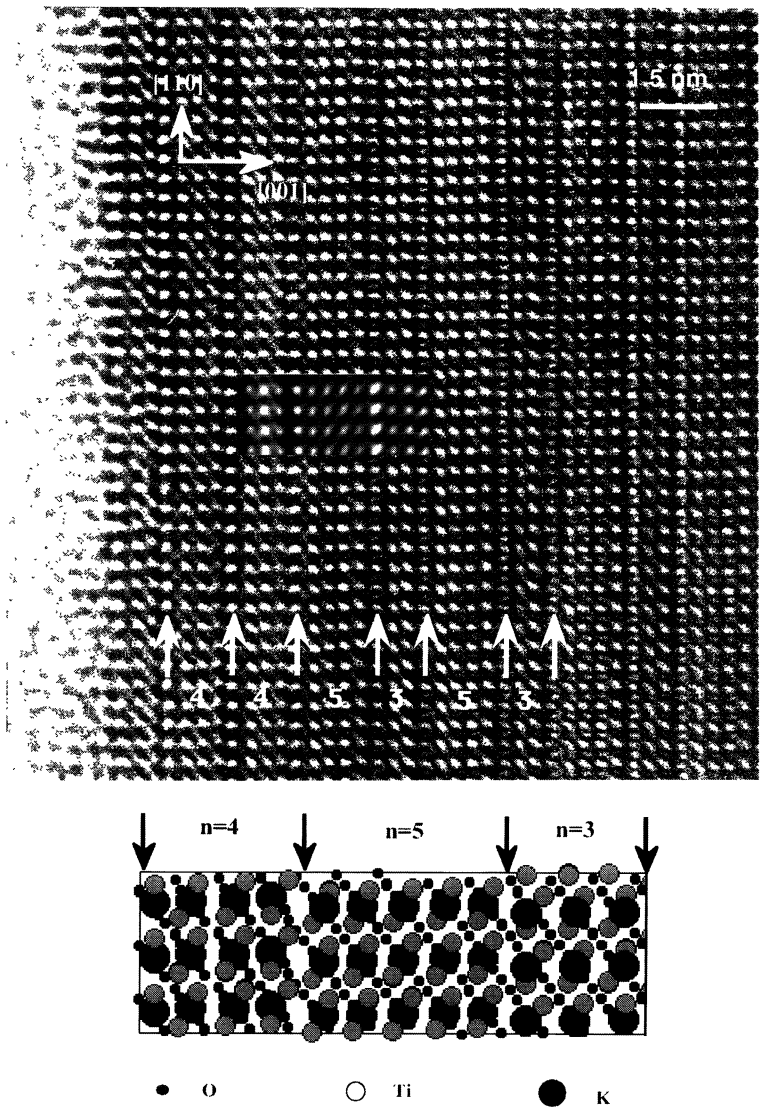

Fig. 24. — [$\bar{1}$10] HREM crystal edge image of HT octatitanate showing LT and HT interface along **c**. Calculated image with $n = 4$, $n = 5$ and $n = 3$ sequences is included as an inset (focus −700 Å and thickness 50 Å). b) Primitive unit mesh along this projecting direction.

The comparison between the HREM observed and simulated images leads to the conclusion that the high temperature form of the octatitanate is built up from a complex sequence consisting of two blocks of 3-steps and 5-steps tunnels titanates respectively. The transformation results in a shift of one upon two interface boundaries in such way that the composition is not modified. The modulus of this shift is one octahedron edge.

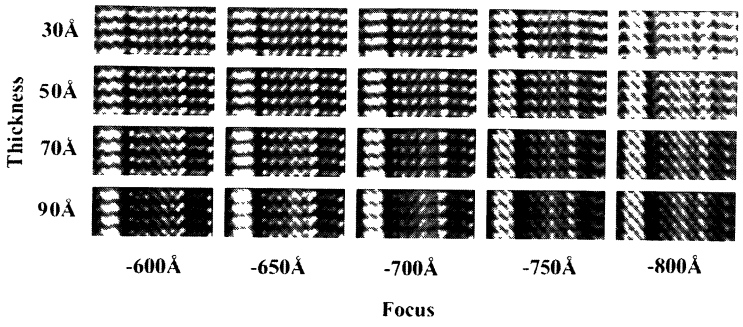

Fig. 25. — Through-focus series of octatitanate with $n = 4$, $n = 5$ and $n = 3$ sequences: focus step −50 Å, thickness step 20 Å.

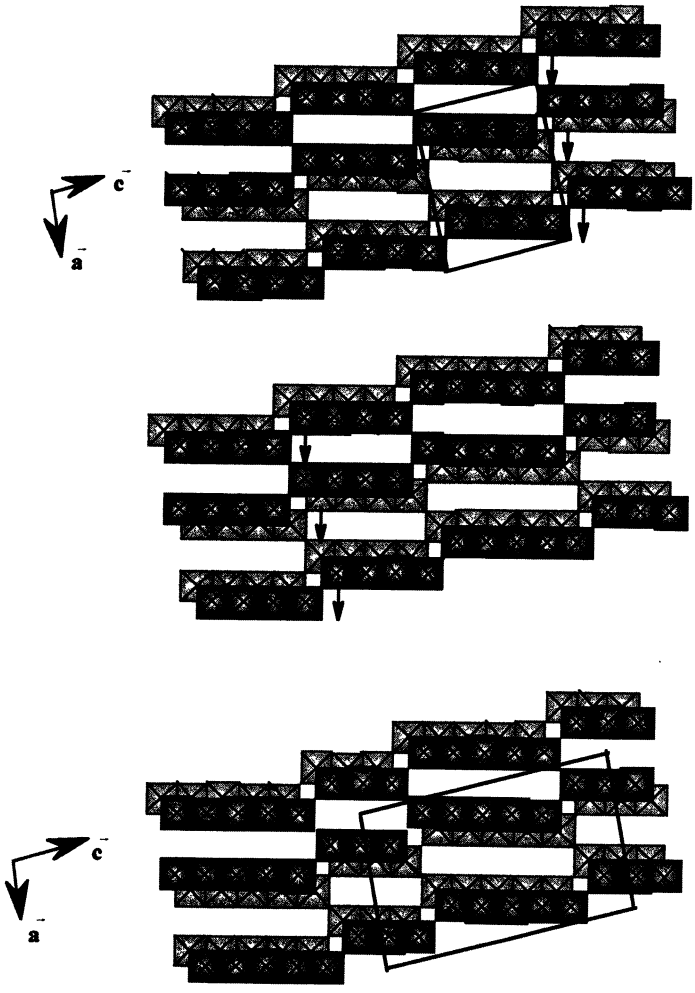

Fig. 26. — Schematic model for the $K_2Ti_8O_{17}$ to $K_4Ti_{16}O_{34}$ transformation. The transformation results in a shift of one upon two interface boundaries.

References

[1] Grey I.E., Madsen I.C., Watts J.A., Bursill L.A. and Kwiatkowska J., *J. Solid State Chem.* **58** (1985) 350.
[2] Wadsley A.D. and Mumme W.G., *Acta Crystallogr. B* **24** (1968) 392.
[3] Watts J.A., *J. Solid State Chem.* **1** (1970) 319.
[4] Marchand R., Brohan L. and Tournoux M., *Mater. Res. Bull.* **15** (1980) 1129.
[5] O'Keefe M.A. and Kilaas R., H.R.E.M. image analysis at the National Center for Electron Microscopy, XIIIth Western Regional Meeting for Electron Microscopy and Microbeam Analysis, Concord, California (1987).
[6] Loiseau A., Van Tendeloo G., Portier R. and Ducastelle F., *J. Phys. France* **46** (1985) 595.
[7] Broddin G., Van Tendeloo G., Van Landuyt J., Amelinckx S., Portier R., Guymont M. and Loiseau A., *Philos. Mag.* **54** (1986) 395.
[8] Planes J., Loiseau A. and Ducastelle F., *J. Phys. I France* **2** (1992) 1507.
[9] Amelinckx S. and Van Dyck D., I.U.G. International Union of Crystallography, Vol. 2, John M. Cowley Ed. (Oxford University Press., 1993) p. 309.
[10] Le Granvalet-Mancini M., Brohan L., Marie A.M. and Tournoux M., *Eur. J. Solid. State Inorg. Chem.* **31** (1994) 767-777.
[11] Hervieu M., Desgardin G. and Raveau B., *J. Solid State Chem.* **30** (1979) 375.
[12] Le Granvalet-Mancini M. and Brohan L., *J. Solid State Chem.* **107** (1993) 127.
[13] Van Tendeloo G., Amelinckx S., Dariet B., Bontchev R., Darriet J. and Weill F., *J. Solid State Chem.* **108** (1994) 314-335.
[14] Duneau M., Du cristal à l'amorphe (Les Éditions de Physique, 1988) pp. 157-197.
[15] Verbaere A., Tournoux M., *Bulletin de la Société Chimique de France* (1973) pp. 1237-1241.
[16] Kilaas R., Mac Tempas V 1.70 and Crystal Kit V1.77, Berkeley.
[17] Reid A.F., Mumme W.G. and Wadsley A.D., *Acta Crystallogr. B* 24 (1968) 1228.